Standing-wave nonlinear optics in an integrated semiconductor microcavity

Alex Hayat* and Meir Orenstein

Department of Electrical Engineering, Technion, Haifa 32000, Israel
**Corresponding author: ahayat@tx.technion.ac.il*

Received July 10, 2007; revised August 9, 2007; accepted August 15, 2007;
posted August 30, 2007 (Doc. ID 85043); published September 27, 2007

We present a concept of standing-wave optical frequency conversion in dispersive microcavities theoretically and experimentally, allowing efficient ultracompact nonlinear photonics. We developed a time-dependent model, incorporating the dispersion into the structure of the spatial cavity modes, where the conversion efficiency is enhanced by the optimization of a nonlinear cavity mode overlap. We designed and fabricated integrated double-resonance semiconductor microcavities for standing-wave second-harmonic generation. The measured efficiency exhibits a significant maximum near the cavity resonance owing to the intracavity power enhancement and the dispersion-induced wavelength detuning effect on the mode overlap, in good agreement with our theoretical predictions.

OCIS codes: 190.4390, 190.4360, 130.5990.

Miniature devices for nonlinear optics [1–5] are of great importance for integrated photonics and quantum information [6–9]. In most of the second-order nonlinear optics experiments, material dispersion is compensated by birefringent crystal phase matching [6] or quasi-phase matching (QPM) [10]. Semiconductors offer a far-reaching alternative due to their high nonlinear susceptibilities and compatibility with the existing photonics technology. However, the main limitation of semiconductor materials is their optical isotropy, which inhibits natural birefringent phase matching, whereas implementation of QPM in semiconductors [2] appears to be difficult. A number of promising methods were developed for semiconductor phase matching, including form birefringence [7,8,11] and modal phase matching [12]. which can be implemented using special materials and processing.

Nonlinear wave mixing in dielectric cavities was recently proposed for materials that cannot be phase matched by conventional means. A properly designed cavity was shown to provide significant process efficiency by phase matching the traveling waves with dispersive dielectric mirrors [5] or using ring microresonators [3]. Moreover, high-quality-factor (Q) cavities can raise the input field amplitudes [13], serve as storage for the produced photons, and generate time separation between exiting photons for photon-number-resolved detection [14].

Here we present a concept of standing-wave optical frequency conversion in dispersive dielectric microcavities theoretically and experimentally. In a standing-wave nonlinear interaction, the conversion efficiency is enhanced by the optimization of a nonlinear mode overlap, allowing the design of miniature devices for efficient cavity nonlinear optics.

For the second-order $\chi^{(2)}$ nonlinear interaction of second-harmonic generation (SHG), the wave equation is [15]

$$\nabla^2 \tilde{E}_2(\mathbf{r},t) = \mu\epsilon \frac{\partial^2 \tilde{E}_2(\mathbf{r},t)}{\partial t^2} + \frac{\chi^{(2)}}{2} \frac{\partial^2 (\tilde{E}_1(\mathbf{r},t))^2}{\partial t^2}, \quad (1)$$

where $\tilde{E}_1(\mathbf{r},t)$ and $\tilde{E}_2(\mathbf{r},t)$ are the pump and the second-harmonic (SH) fields, respectively.

In contrast to the usual approach of traveling-wave phase matching [1–12,16], our concept is based on the interaction between spatial cavity eigenmodes in a slowly time-varying envelope approximation. Therefore the pump and the SH fields are written as

$$\tilde{E}_1(\mathbf{r},t) = E_1(t) e^{i\omega_1 t} F_1(\mathbf{r}),$$

$$\tilde{E}_2(\mathbf{r},t) = E_2(t) e^{i\omega_2 t} F_2(\mathbf{r}), \quad (2)$$

where $F_i(\mathbf{r})$ are the orthonormal set of spatial cavity modes, assumed to be unaffected by the weak nonlinear interaction and $E_i(t)$ are the slowly time-varying envelopes relative to the oscillation period $T = 2\pi/\omega$, for which the approximation $\partial E(t)/\partial t T \ll E(t)$ can be applied. These approximations are analogous to the slowly varying spatial envelope and the unmodified transversal mode approximations, usually employed in traveling-wave nonlinear optics [15]. Therefore, assuming $|\partial^2 E_2(t)/\partial t^2| \ll |\omega_2 \partial E_2(t)/\partial t|$ for the slow time-envelope approximation, and using a strong undepleted pump $E_1(t)$, the wave equation is

$$E_2(t) e^{i\omega_2 t} \nabla^2 F_2(\mathbf{r}) = \mu\epsilon_2 \left[2i\omega_2 \frac{\partial E_2(t)}{\partial t} - \omega_2^2 E_2(t) \right] e^{i\omega_2 t} F_2(\mathbf{r}) - \mu \frac{\chi^{(2)}}{2} \omega_2^2 E_1^2(t) e^{i\omega_2 t} F_1^2(\mathbf{r}), \quad (3)$$

where ϵ_i are the dielectric constants. To calculate the

0146-9592/07/192864-3/$15.00

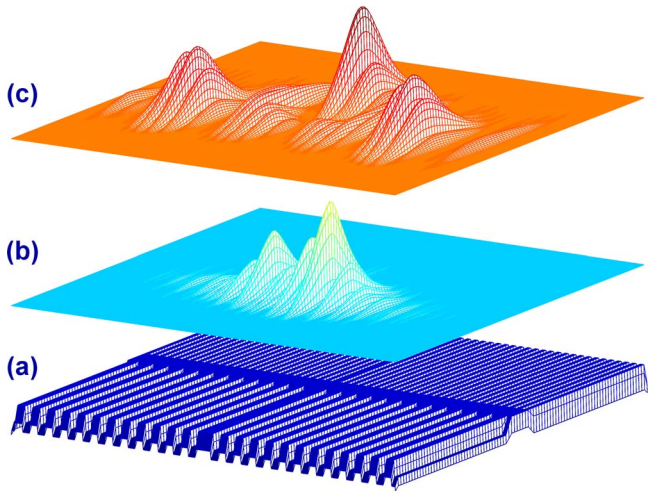

Fig. 1. (Color online) (a) Schematic drawing of the integrated double-resonance microcavity. (b) Calculated (FDTD) SH cavity mode two-dimensional intensity distribution in the QW region (arb. u.). (c) Calculated (FDTD) pump cavity mode two-dimensional intensity distribution in the QW region (arb. u.).

time dependence of the SH mode envelope, the equation is multiplied by $F_2^*(\mathbf{r})$ and integrated spatially yielding

$$\frac{\partial E_2(t)}{\partial t} = \frac{1}{2i}\left[\frac{\int d\mathbf{r} F_2^*(\mathbf{r})\nabla^2 F_2(\mathbf{r})}{\mu\epsilon_2\omega_2} + \omega_2\right]E_2(t) + \frac{i\gamma\chi^{(2)}\omega_2}{4\epsilon_2}E_1^2(t), \quad (4)$$

where $\gamma = \int d\mathbf{r} F_2^*(\mathbf{r}) F_1^2(\mathbf{r})$ is the nonlinear mode overlap.

The first term on the right-hand side of Eq. (4) represents the radiative cavity losses, which can be designated by $-\alpha/2E_2(t)$, and thus

$$\frac{\partial E_2(t)}{\partial t} = \frac{i\gamma\chi^{(2)}\omega_2}{4\epsilon_2}E_1^2(t) - \frac{\alpha}{2}E_2(t). \quad (5)$$

This time dependence of the SH mode field stems from the converted intracavity field buildup limited only by the cavity optical loss term α, where the spatial cavity modes overlap; γ provides the local presence of the electromagnetic fields necessary for the nonlinear interaction.

Applying zero initial condition for the SH field, the $E_2(t)$ envelope time dependence (for a constant pump) is:

$$E_2(t) = \frac{i\gamma\chi^{(2)}\omega_2}{2\epsilon_2\alpha}E_1^2(1 - e^{-\alpha/2t}), \quad (6)$$

and at steady state, the pump and SH powers are related by

$$P_2 = \frac{1}{\epsilon_2\epsilon_1^2}\left|\frac{\gamma\chi^{(2)}\omega_2}{2\alpha}\right|^2 P_1^2. \quad (7)$$

Hence in a properly designed cavity, with a large mode overlap γ and a small cavity loss term α, the nonlinear process can be enhanced significantly, regardless of the device dimensions. An important parameter of the standing-wave nonlinear interaction is the cavity Q factor, which determines both the cavity losses and the operation bandwidth. A nonlinear device based on high-Q microcavity can significantly enhance the performance at the designed wavelength, however, with narrowband conversion efficiency.

We designed an integrated double-resonance microcavity according to the model described above, applying two one-dimensional photonic crystal cavities for the pump and the SH fields. The two structures were applied—one on the left side and the other on the right side—of a 4-μm-wide 0.4-μm-high AlGaInP ridge waveguide [Fig. 1(a)] with 4 GaInP quantum well (QW) layers. The cavity was engineered to have resonances at the 1512 nm pump and 756 nm SH wavelengths, using three-dimensional finite-difference time-domain (FDTD) simulations taking into consideration the effect of material dispersion. Spatial cavity mode field distributions $F_1(\mathbf{r})$ and $F_2(\mathbf{r})$ were also calculated by the FDTD simulations [Figs. 1(b) and 1(c)].

The actual cavities were fabricated on samples consisting of four periods of compressively strained 50 Å $Ga_{0.45}In_{0.55}P$ QWs separated by 55 Å $(Al_{0.5}Ga_{0.5})_{0.51}In_{0.49}P$ barriers. The lateral light confinement was achieved by a 4-μm-wide ridge waveguide, realized by etching techniques. The integrated 10-μm-long double-resonance microcavities were implemented by milling the periodic structure using a FEI Strata 400 Focused Ion Beam system (Fig. 2).

The structure was optically pumped by 130 fs pulses at telecommunication wavelengths (1500–1530 nm) far from the two-photon absorption wavelengths of $Ga_{0.45}In_{0.55}P < 1340$ nm using an opti-

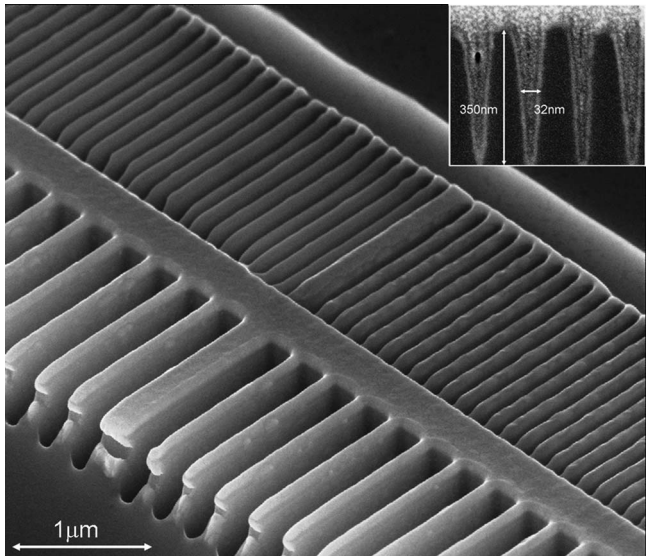

Fig. 2. Scanning electron microscopy (SEM) image of the fabricated integrated double-resonance microcavity. The inset is a SEM cross-section image of the shortest period grating.

cal parametric oscillator (OPO), which was pumped by a mode-locked Ti:Sp fs laser at 810 nm. The OPO output was facet coupled into the waveguide with about 2 μm^2 mode area by a polarization maintaining lensed fiber, after filtering out the residual Ti:Sp 810 nm pump by a thick GaAs wafer with average pump power of ~100 mW. The generated SH was fiber coupled into a spectrum analyzer with an optical output, and the photon detection was performed by a Perkin-Elmer photon counting module, SPCM 14. The measured efficiency, $P_{out}/P_{in}{}^2$, shows a significant maximum near the cavity resonance at ~1512 nm [Fig. 3(a)].

The cavity linear transmission spectrum [Fig. 3(a) inset] corresponds to a relatively low Q factor (Q <100), which is sufficient, however, to demonstrate standing-wave nonlinear interaction. Due to fabrication imperfections (e.g., milling depth and width variations) the measured transmission spectrum is slightly wider than the calculated one, having a longer wavelength sidelobe near ~1520 nm. The linear cavity spectrum is related directly to the nonlinear conversion efficiency spectrum, resulting in a sidelobe at ~1520 nm in the nonlinear response.

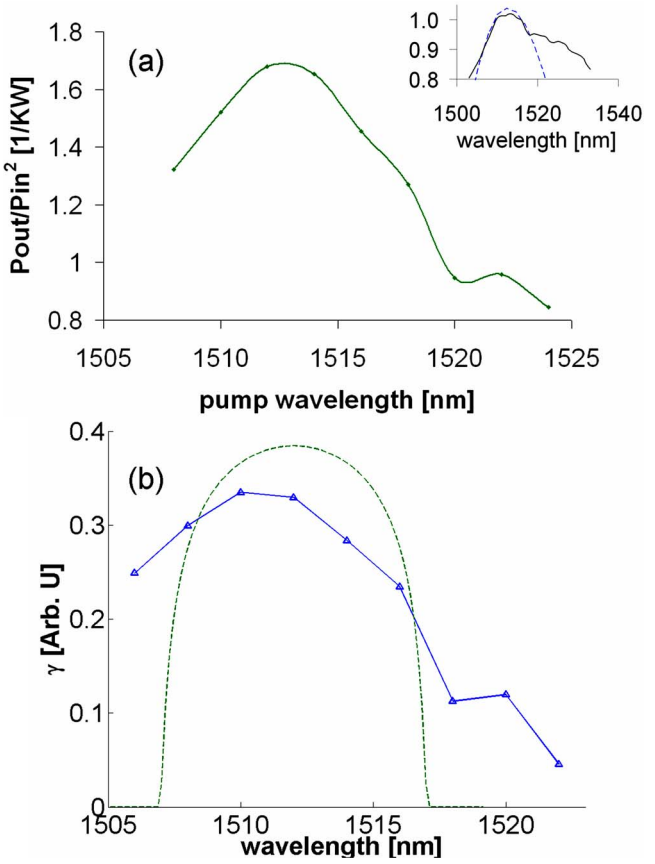

Fig. 3. (Color online) (a) Measured SH generation efficiency $P_{out}/P_{in}{}^2$ wavelength dependence. The inset is the microcavity transmission spectrum around the 1512 nm resonance. The solid curve is the measured and the dashed curve is the calculated (FDTD) spectrum. (b) Nonlinear mode overlap γ wavelength dependence. The solid curve is the measured and the dashed curve is the calculated spectrum.

The effect of wavelength detuning on the nonlinear mode overlap was analytically estimated for a one-dimensional photonic crystal cavity using coupled-mode theory for the fields in the grating regions. The grating complex mode-propagation constant is [15]

$$\beta' = \beta_0 \pm i\sqrt{\kappa^2 - (\Delta\beta)^2}, \tag{8}$$

where the detuning $\Delta\beta = \beta(\omega) - \beta_0 = \beta(\omega) - \pi/\Lambda$, Λ is the grating period, and κ is the grating coupling constant. Detuned operation results in slow spatial field decay in the grating region, and thus significant parts of the cavity modes exhibit oscillatory behavior. Gratings for the pump and the SH fields were designed considering dispersion, and spatially oscillating parts of the normalized modes cause a smaller nonlinear mode overlap for weaker field decay in the grating regions with increasing detuning. The nonlinear mode overlap γ, therefore, has a maximum for $\Delta\beta = 0$ and vanishes for $|\Delta\beta| > |\kappa|$ [Fig. 3(b)]. The measured γ wavelength dependence extracted by using Eq. (7) clearly resembles the calculated one.

In conclusion, we modeled, designed, and fabricated integrated double-resonance semiconductor microcavities for standing-wave SHG. Our experimental results show a strong maximum in the measured SHG efficiency near the cavity resonances owing to the increased input power and the wavelength detuning effect on the nonlinear mode overlap, matching our theoretical predictions.

References

1. S. Venugopal Rao, K. Moutzouris, and M. Ebrahimzadeh, J. Opt. A **6**, 569 (2004).
2. D. Artigas, E. U. Rafailov, P. Loza-Alvarez, and W. Sibbett, IEEE J. Quantum Electron. **40**, 1122 (2004).
3. Z. Yang, P. Chak, A. D. Bristow, H. M. van Driel, R. Iyer, J. S. Aitchison, A. L. Smirl, and J. E. Sipe, Opt. Lett. **32**, 826 (2007).
4. P. Herskind, J. Lindballe, C. Clausen, J. L. Sørensen, and M. Drewsen, Opt. Lett. **32**, 268 (2007).
5. G. Klemens, C.-H. Chen, and Y. Fainman, Opt. Express **13**, 9388 (2005).
6. P. G. Kwiat, K. Mattle, H. Weinfurter, A. Zeilinger, A. V. Sergienko, and Y. Shih, Phys. Rev. Lett. **75**, 4337 (1995).
7. G. Leo and E. Rosencher, Opt. Lett. **23**, 1823 (1998).
8. L. Lanco, S. Ducci, J. P. Likforman, X. Marcadet, J. A. W. van Houwelingen, H. Zbinden, G. Leo, and V. Berger, Phys. Rev. Lett. **97**, 173901 (2006).
9. J. Jing, S. Feng, R. Bloomer, and O. Pfister, Phys. Rev. A **74**, 041804(R) (2006).
10. K. Banaszek, A. B. U'Ren, and I. A. Walmsley, Opt. Lett. **26**, 1367 (2001).
11. A. Fiore, V. Berger, E. Rosencher, P. Bravetti, and J. Nagle, Nature **391**, 463 (1998).
12. A. De Rossi, V. Berger, G. Leo, and G. Assanto, IEEE J. Quantum Electron. **41**, 1293 (2005).
13. Z. Y. Ou and Y. J. Lu, Phys. Rev. Lett. **83**, 2556 (1999).
14. A. Hayat and M. Orenstein, Appl. Phys. Lett. **89**, 171108 (2006).
15. A. Yariv, *Optical Electronics in Modern Communications* (Oxford U. Press, 1997).
16. A. Fiore, E. Rosencher, V. Berger, and J. Nagle, Appl. Phys. Lett. **67**, 3765 (1995).